Fibrillar Structure of Self-Assemblies Formed from Heterocomplementary Monomers Linked through Sextuple Hydrogen-Bonding Arrays

E. BUHLER,[1,2] S. J. CANDAU,[3] J. SCHMIDT,[4] Y. TALMON,[4] E. KOLOMIETS,[3] J.-M. LEHN[3]

[1]Laboratoire de Spectrométrie Physique, UMR CNRS 5588, Université Joseph Fourier de Grenoble, 38402 St. Martin d'Hères, France

[2]Laboratoire Matière et Systèmes Complexes, UMR CNRS 7057, Université Paris 7-Denis Diderot, 75251 Paris Cedex 05, France

[3]I.S.I.S., Laboratoire de Chimie Supramoléculaire, UMR CNRS 7006, ISIS-Université Louis Pasteur, 67083 Strasbourg Cedex, France

[4]Department of Chemical Engineering, Technion-Israel Institute of Technology, Haifa 32000, Israel

Received 27 May 2006; revised 1 August 2006; accepted 20 August 2006
DOI: 10.1002/polb.20960
Published online in Wiley InterScience (www.interscience.wiley.com).

ABSTRACT: The nanostructure of the fibrillar supramolecular aggregates generated in decane solutions of homoditopic heterocomplementary monomers forming sextuple hydrogen-bond-mediated self-assemblies was investigated by small-angle neutron scattering and cryogenic-temperature transmission electron microscopy. The persistence length (L_p) of the fibrillar aggregates was found to be ~18 nm, as inferred from combined measurements of the radius of gyration and of the contour length. The values of both the weight-average molecular weight and the mass per unit length of the fibers suggest that the latter consist of few aggregated monomolecular wires. At $T = 25$ °C, the formation of branched aggregates occurs around the crossover concentration, C^*, between the dilute and semidilute regimes, whereas the classical behavior of equilibrium polymers is observed at $T = 65$ °C. ©2006 Wiley Periodicals, Inc. J Polym Sci Part B: Polym Phys 45: 103–115, 2007
Keywords: cryo-TEM; hydrogen-bond-mediated self-assemblies; neutron scattering; structure; supramolecular polymers

INTRODUCTION

The molecular recognition-directed association between monomers bearing complementary hydrogen bonding groups leads to linear supramolecular polymers.[1–38] The formation of such reversible polymers from monomers linked through sextuple hydrogen-bonding arrays has been recently reported.[17,38] The strong affinity of the DAD-DAD (D = donor, A = acceptor) hydrogen-bonding sites for double-faced cyanuric acid type ADA-ADA wedges drives the supramolecular polymeric assembly in organic solvents of low polarity as shown in Figure 1, where the bisreceptor AA9 bearing decanoyl side chains is associated with the biswedge BB.

A recent small-angle neutron scattering (SANS) study showed that such monomers in decane solutions self-assemble into long rigid or semirigid rods whose length increases upon increasing monomer

Correspondence to: J.M. Lehn (E-mail: lehn@isis.u-strasbg.fr)

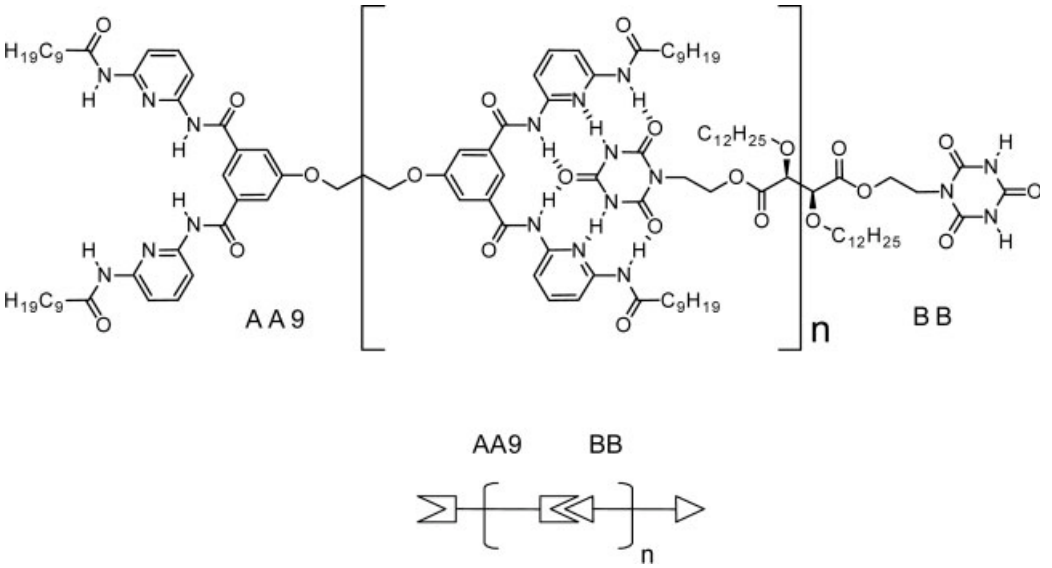

Figure 1. Linear supramolecular polymer [AA9:BB]$_n$ formed by H-bond-mediated molecular recognition between heterocomplementary binding sites of homoditopic bis-receptor AA9 and homoditopic biswedge BB.

concentration and/or decreasing temperature.[38] The cross section and the linear density of these rods were found to be constant over large concentration and temperature ranges and of the order of 10 nm^2 and 5150 g mol^{-1} nm^{-1}, respectively. The latter value is much larger than that expected for straight monomolecular wires for which the linear density would be 480 g mol^{-1} nm^{-1}.

This difference was explained by assuming a stacking of the disk-shaped aromatic rings of the molecules. Two possible superstructures were envisioned. The first one involved a molecular folding with interpenetration of two chains, the second one an intermolecular stacking of ~10 extended monomolecular chains leading to the formation of possibly helicoidal ribbons. It is also worth stressing that the experimental values of the structural characteristic parameters were reproducible and independent of concentration and temperature, which suggests a well-defined superstructure of the self-assemblies.

Beyond the critical rod overlap concentration C^*, the systems become highly viscous and at concentrations $C > 4C^*$, exhibit features of physical gels.

A surprising result concerns the behavior in the vicinity of C^*, where a huge increase of both the correlation length and the scattered intensity is observed, whereas a smooth maximum is expected. To explain these results, it was speculated that, close to C^*, the rodlike particles become interconnected to form highly branched aggregates as in percolating systems. These aggregates were found to break upon increasing temperature, but this effect could be due to a shift of C^* to a higher value.

In attempting to clarify the above issue, we performed SANS experiments on systems with concentrations ranging on both sides of C^* at $T = 65$ °C. We have also determined the scattering curve for a sample with $C = 1$ mM as a function of temperature. By combining the measurements of scattered intensity at low scattering angle and of the mass per unit length, we determined the variations of the average length of the fibrillar species as a function of the temperature and concentration. An estimate of the persistence length was obtained from the comparison of the radius of gyration and the length of the fibrils. Also, the branched structure previously suggested for the systems in the vicinity of C^* at $T = 25$ °C could be assessed unambiguously.

Electron microscopy experiments performed by means of either direct observation or cryofracturing techniques on similar systems were previously reported.[17] The obtained micrographs show the formation of long, sometimes helical, fibers with a cross section much larger than that measured in SANS experiments. Obviously, these large objects do not reflect exactly the structure of the self-assemblies formed in the solutions, because of the perturbations produced by the method of film preparation. In the present study, we have employed the

cryogenic-temperature transmission electron microscopy (cryo-TEM) technique that is a less invasive method.[39,40]

The solvent used for these experiments is the Isopar M that is an industrial compound consisting of a mixture of branched paraffins of the kind $(CH_3)_2—CH—(CH_2)_n—CH_3$ with n around 9 and 10. This solvent can be vitrified in liquid nitrogen (the cryogen of choice, liquid ethane dissolves hydrocarbons), whereas linear paraffins crystallize.[41] The structure of the fibers observed in the micrographs obtained with these samples is compared with that inferred from the SANS results.

EXPERIMENTAL

Sample Characteristics

The synthesis of the homoditopic receptor AA9 and the ditopic substrate BB, whose formula are given in Figure 1 has been described in a previous publication.[38]

Bisreceptor AA9 and biswedge BB are almost insoluble in decane as individual compounds. In contrast, their mixtures in 1:1 stoichiometry dissolve readily in decane under heating to form transparent solutions that are stable over time and thermal cycles. A sharp increase of viscosity is observed at the crossover concentration, C^*, between dilute and semidilute regimes, that is, the concentration beyond which the polymeric aggregates start to overlap.

The crossover concentration C^* was determined from viscosimetric measurements and found to be $\sim$2.2 mM at $T = 25$ °C and $\sim$3.5 mM at $T = 65$ °C. Solutions in deuterated decane were prepared for SANS experiments in the concentration range 0.5–10 mM (0.109×10^{-2} – 2.18×10^{-2} g cm^{-3}), that is, on both sides of C^*.

The samples used for electron microscopy experiments were solutions in Isopar M at concentrations $C = 1$ and 2 mM. Isopar M is a narrow cut isoparaffinic mixture from Esso Chemie (boiling range 207–257 °C, molar volume 244.9 cm^3). The predominant species are branched paraffins $(CH_3)_2—CH—(CH_2)_n—CH_3$ with $n \sim 9$–10. These solutions were not studied by viscosimetry but visual observations indicate that the crossover concentration, C^*, is slightly lower than that in decane solutions 1 mM $< C^* <$ 2 mM at $T = 25$ °C. This suggests an enhanced polymeric growth upon increasing concentration.

Small-Angle Neutron Scattering

SANS experiments were carried out on the PACE spectrometer in Léon Brillouin Laboratory at Saclay (LLB, France). The chosen incident wavelength, λ, depends on the set of experiments, as follows. For a given wavelength, the range of the amplitude of the transfer wavevector q was selected by changing the detector distance, D. Three sets of sample-to-detector distances and wavelengths were chosen [$D = 1$ m, $\lambda = (6 \pm 0.5)$ Å; $D = 4.68$ m, $\lambda = (6 \pm 0.5)$ Å; and $D = 4.68$ m, $\lambda = (17 \pm 1.5)$ Å] so that the following q-ranges were respectively, available: $3.62 \times 10^{-2} \leq q$ (Å^{-1}) $\leq 3.68 \times 10^{-1}$, $6.9 \times 10^{-3} \leq q$ (Å^{-1}) $\leq 7.35 \times 10^{-2}$, and $2.42 \times 10^{-3} \leq q$ (Å^{-1}) $\leq 2.58 \times 10^{-2}$. Measured intensities were calibrated to absolute values (cm^{-1}), using normalization by the attenuated direct beam classical method. Standard procedures to correct the data for the transmission, detector efficiency, and backgrounds (solvent, empty cell, electronic, and neutronic background) were carried out. The scattered wavevector, q, is defined by eq 1, where θ is the scattering angle.

$$q = \frac{4\pi}{\lambda} \sin\frac{\theta}{2} \tag{1}$$

The usual equation for absolute neutron scattering combines the intraparticle scattering $S_1(q) = V_{\text{chain}}\phi_{\text{vol}}P(q)$ form factor with the interparticule scattering $S_2(q)$ factor:

$$\begin{aligned} I(q)(\text{cm}^{-1}) = \frac{1}{V}\frac{\mathrm{d}\sigma}{\mathrm{d}\Omega} &= (\Delta\rho)^2(S_1(q) + S_2(q)) \\ &= (\Delta\rho)^2(V_{\text{chain}}\phi_{\text{vol}}P(q) + S_2(q)) \end{aligned} \tag{2}$$

where $(\Delta\rho)^2 = (\rho_{\text{monomer}} - \rho_{\text{solvent}})^2$ is the contrast per unit volume between the polymer and the solvent, which was determined from the known chemical composition. $\rho = \Sigma n_i b_i/(\Sigma n_i m_i v \times 1.66 \times 10^{-24})$ represents the scattering length per unit volume; b_i is the neutron scattering length of the species i; m_i the mass of species i, and v the specific volume of the monomer (which has been taken to be equal to 1 cm^3 g^{-1}), or the solvent (i.e., 1.1834 cm^3 g^{-1} for deuterated decane). $P(q)$ is the form factor, $V_{\text{chain}} = Nvm \times 1.66 \times 10^{-24}$ is the volume of the N monomers (of mass m) in a chain, and ϕ_{vol} is the volume fraction of monomer. In the high q-range, the scattering is assumed to arise from isolated chains, that is $S_2(q) = 0$, and thus $I(q) \propto P(q)$.

In the course of the study, we also report some data obtained in a previous set of measurements carried out on the spectrometer D11 at Laue Langevin Institut at Grenoble (ILL, France) at $T = 25$ and 65 °C.[38]

Cryogenic-Temperature Transmission Electron Microscopy

Vitrified specimens for cryogenic-temperature transmission electron microscopy (Cryo-TEM) were prepared in a controlled environment vitrification system (CEVS) at 25 °C and 100% relative solvent saturation, as previously described.[39,40] In brief, a drop of the solution to be imaged was applied onto a perforated carbon film, supported on an electron microscopy copper grid, held by the CEVS tweezers. The sample was blotted by filter paper, and immediately plunged into liquid nitrogen (−196 °C). The vitrified samples were then stored under liquid nitrogen, transferred to a Gatan 626 cooling holder via its "work station," and kept in a FEI T12 G^2 microscope at about –180 °C. Images were recorded at 120 kV acceleration voltage, in the low-dose mode, to minimize electron-beam radiation-damage. We used a Gatan UltraScan 1000 high-resolution cooled-CCD camera, with the Digital Micrograph software package, to acquire the images. Images were recorded at nominal underfocus of about 1–2 μm to enhance phase-contrast.

RESULTS

Small-Angle Neutron Scattering Studies

Figure 2 displays the scattering patterns for $[AA9:BB]_n$ solutions in deuterated decane at various concentrations spanning both dilute and semidilute regimes at $T = 65$ °C. For clarity, the representation $I(q) \times C$ was chosen to shift the curves with respect to each other. All the scattering curves exhibit the same overall behavior, characterized by the following sequence: a Guinier regime in the low q range associated with the finite size of the scattering objects, one intermediate regime in which the q dependence of the scattered intensity can be described by a power law with an exponent close to −1, a Guinier regime at higher q corresponding to the cross section of the fibers, and eventually a dip which is the initial part of the oscillating term of the shape-dependent form factor of the particle cross section. In the vicinity of C^*, one does not observe any significant upturn of the scattering intensity in the low q range, contrary to the pre-

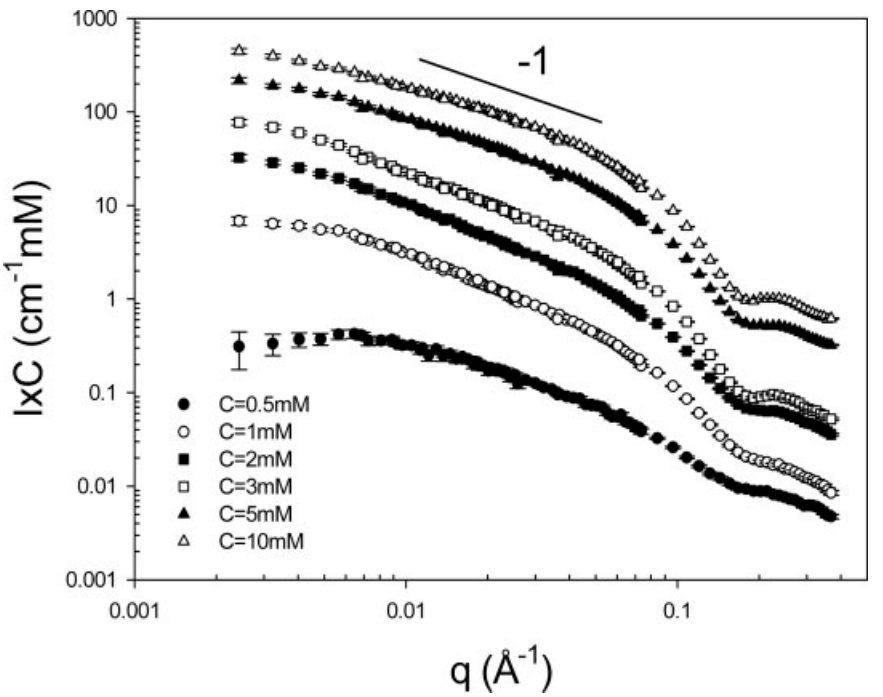

Figure 2. Scattering patterns for $[AA9:BB]_n$ solutions in deuterated decane at various concentrations at $T = 65$ °C. For clarity, the representation $I(q) \times C$ was chosen to shift the curves with respect to each other.

viously reported behavior at $T = 25$ °C. This is also illustrated by Figure 3 that shows the concentration dependence of the ratio of the low q scattered intensity over the concentration, $I(q = 0)/C$, at $T = 25$ and 65 °C, respectively. The variation of $I(q = 0)/C$ at $T = 65$ °C exhibits a smooth maximum, whereas a sharp peak is observed at $T = 25$ °C around C^*. Also, the scattering intensity at the maximum is about 10^3 times larger at 25 °C than that at 65 °C. At high concentrations, the variations of the scattered intensity with concentration tend to coincide, within the experimental accuracy, as in semidilute solutions of conventional polymers.

Figure 4 shows the scattering curves obtained for a sample with $C = 1$ mM at $T = 45$ and 65 °C, respectively. The decrease of scattered intensity at low q upon increasing temperature indicates a breaking of the polymeric particles, but the local structure remains unaltered as proved by the superposition of the scattering curves in the intermediate and high q range. Similar results were obtained for the sample at $C = 2$ mM.

Cryo-TEM

As mentioned above, we had to substitute decane with Isopar M, a mixture of branched hydrocarbons that can be vitrified in liquid nitrogen. The nanostructures in the vitrified specimens revealed by direct-imaging cryo-TEM are not unlike thread-like micelles (TLMs) that we have studied extensively in aqueous media, for example, Refs. [42] and [43]. As is quite common in nonaqueous systems, the contrast of the chains relative to the continuous phase is much lower than what is observed in aqueous solutions.[44] This is true even when some of the water is replaced by water-soluble organic material such as ethylene glycol or glycerol.[43] Another difficulty is the very high sensitivity of such specimens to the electron beam. We used low-dose imaging to minimize the number of electrons used to record an image to less than 20 $e^-/Å^2$. Higher exposures may lead to loss or reversal of contrast,[44] and to loss of details.

Because of the high depth-of-field of the TEM, all the structures in the thin specimens are projected, focused, on the detector. This makes data interpretation difficult due to the overlap of information. The two images in Figure 5 show the structures formed by the $[AA9:BB]_n$ system. The structure seen in Figure 5(a) at 1 mM and in Figure 5(b) at 2 mM is quite similar. Because of information overlap and somewhat different thickness, and occasional redistribution of the aggregates, it is hard to tell the difference in concentration. Note that some of the aggregates are branched (white arrows), not unlike certain

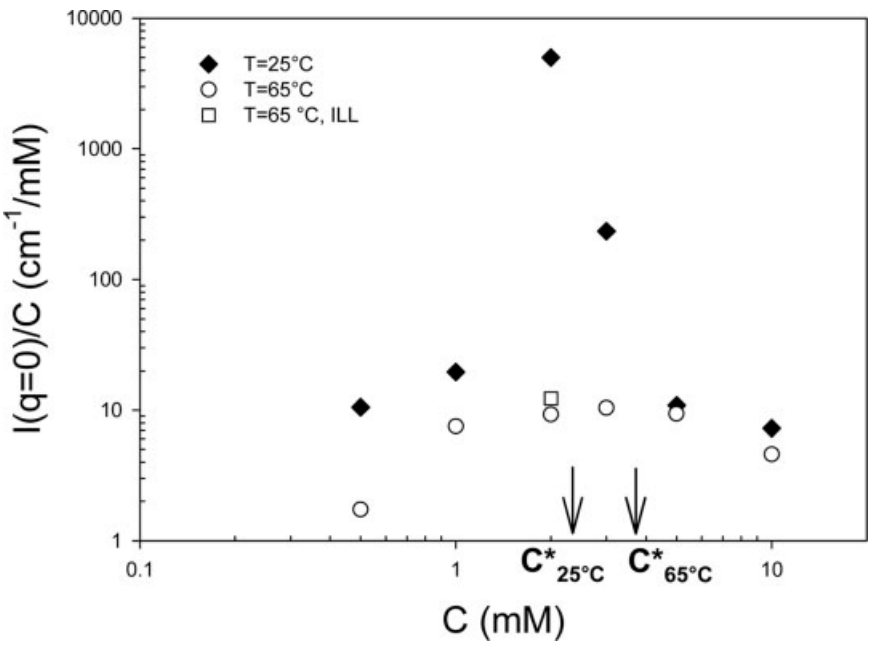

Figure 3. Concentration dependence of the ratio of the scattered intensity at zero-wave vector over C, $I(q = 0)/C$, at $T = 25$ °C (◆) and $T = 65$ °C (○). Data obtained in a previous set of measurements performed at ILL are also reported (□).[38]

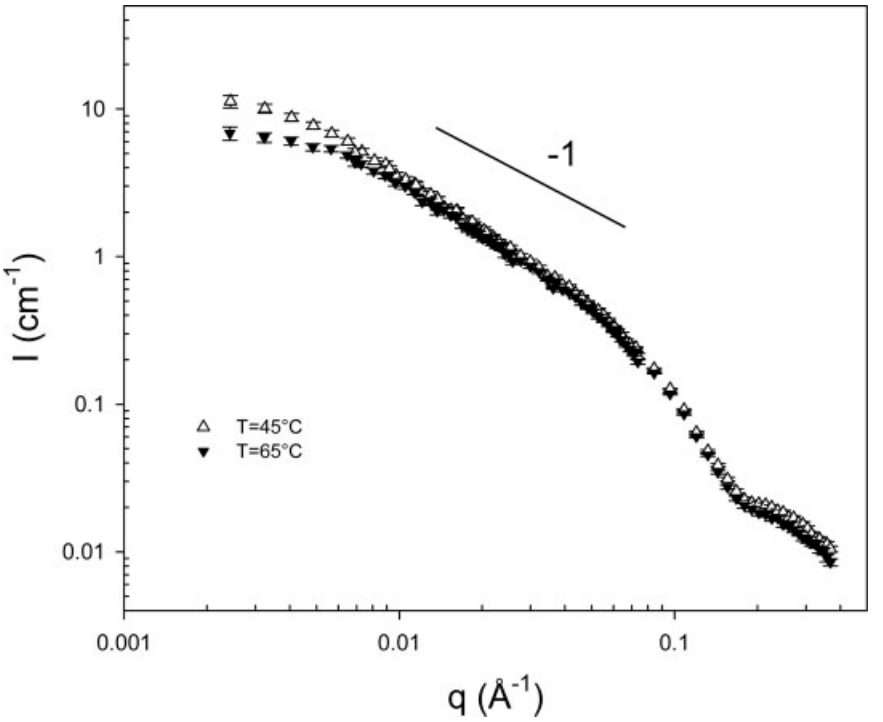

Figure 4. SANS spectra obtained for a 1 mM solution of $[AA9:BB]_n$ at $T = 45$ °C (△) and 65 °C (▼) in decane.

TLM systems.[43] The apparent small dark dots [black arrows in Fig. 5(a)] are projections of segments, especially end-segments, of the aggregates, aligned parallel to the electron beam.

Electron microscopy is an excellent tool to identify the morphology of the building blocks in the systems. As such it gives us a direct, model-independent, picture of the system, showing that it is made of threadlike, occasionally branched aggregates. But cryo-TEM is not a very accurate quantitative tool, because magnification is very sensitive to the position of a given area of the specimen along the optical axis. Nevertheless, we can estimate the tranverse dimension of the aggregates to be 3.5 ± 0.5 nm, which is in agreement with the value deduced for the cross section of the aggregates, 10 nm^2. Because of nanostructure overlap, it is impossible to determine the overall length of the aggregates.

DISCUSSION

Local Conformation

In the intermediate q regime, the scattering curves can be fitted satisfactorily by a rigid rod model. Figure 6 shows the fits realized for a 2 mM solution of $[AA9:BB]_n$, that is in the dilute regime, by means of the des Cloizeaux law[45] derived for rigid rod particles and valid for $qL_p > 2$, where L_p is the persistence length and L the contour length.

$$P(q) = \frac{\pi}{qL} + \frac{2}{3q^2L_pL} \tag{3}$$

The high q data can be fitted by a Guinier expression for the form factor of the section:

$$V_{chain}P(q) = \frac{\pi S}{q} \exp\left(-q^2r_c^2/2\right) \tag{4}$$

where r_c is the radius-of-gyration of the cross section. By fitting the two above equations to the experimental data, one can determine the mass per unit length of the fibrillar aggregates, M_l, the section, S, and the radius of gyration, r_c, of the cross section. From the fits of Figure 6, we obtain $M_l = 5180\ g\ mol^{-1}\ nm^{-1}$, $S = 11.3\ nm^2$, and $r_c = 1.4$ nm. A statistical analysis of the scattering curves obtained for all concentrations investigated, at both $T = 25$ and 65 °C temperatures, lead to the following values of the structural parameters: $M_l = 5200 \pm 500\ g\ mol^{-1}\ nm^{-1}$, $S = 10.8 \pm 0.5\ nm^2$, and $r_c = 1.5 \pm 0.2$ nm.

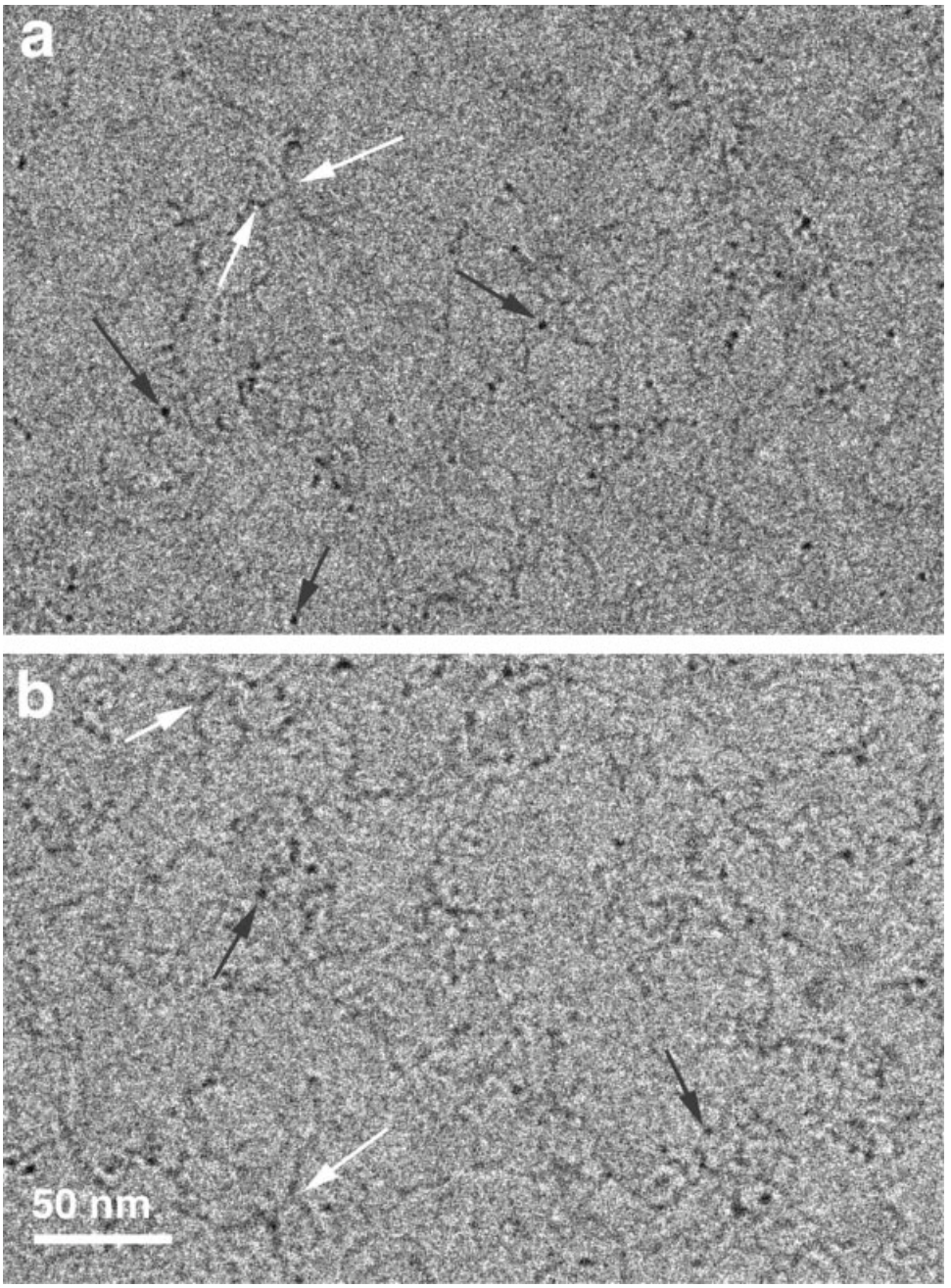

Figure 5. Cryo-TEM images at $C = 1$ mM (a) and $C = 2$ mM (b) $[AA9:BB]_n$ solutions in Isopar M in the vicinity of C^*. Note branching (white arrows) and end-segments aligned parallel to the electron beam (black arrows).

It must be underlined that the two series of experiments, performed either at two locations (ILL or LLB, see Experimental section) concern two different preparations with different aging of the samples; this shows that the monomers self-assemble into aggregates with well-defined structure.

Overall Molecular Conformation

The low q data have been fitted by the Ornstein–Zernicke law:

$$\frac{1}{I(q)} = \frac{1}{I(0)}(1 + q^2\xi^2) \qquad (5)$$

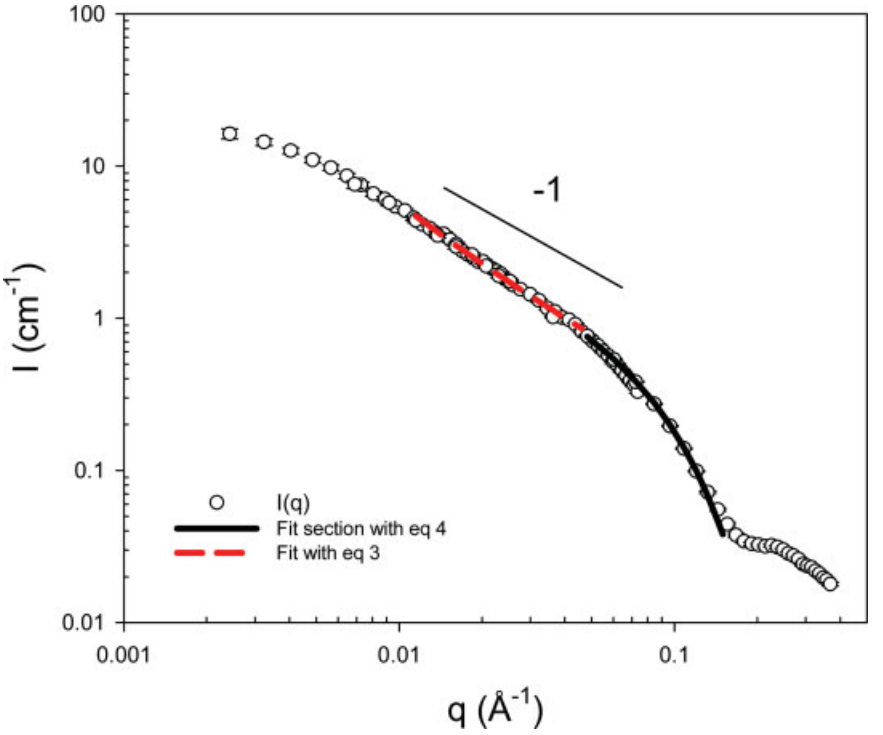

Figure 6. SANS spectra obtained for a 2 mM solution of $[AA9:BB]_n$ at 65 °C in decane. The dashed line represents the fit of the data in the intermediate regime with eq 3, and the black line represents the fit of the high q data by a Guinier expression for the form factor of the section (eq 4). [Color figure can be viewed in the online issue, which is available at www.interscience.wiley.com.]

where ξ is the correlation length. In the dilute range, the radius of gyration of the particle is given by $R_G = 3^{1/2} \times \xi$. Figure 7(a) shows the comparison between the concentration dependence of the correlation length obtained at $T = 25$ and 65 °C, respectively. The variations of ξ are strongly correlated to those of the scattered intensity shown in Figure 3. At $T = 65$ °C, the behavior of $I(q = 0)$ is quite similar to that observed for other equilibrium polymers, namely, a significant increase with concentration in the dilute range, followed by a smooth maximum in the vicinity of C^*, then by a decrease in the semidilute regime. At $T = 25$ °C, a large unexpected increase of the scattered intensity is observed close to C^*. Such behavior is the signature of the formation of branched aggregates rather than that of a huge linear polymeric chain as discussed later on in this study. Indeed, branched aggregates are observed in the microphotographs of Figure 5. From the measured values of $I(q = 0)$ and of the mass per unit length, M_l, it is possible to determine the average contour length of the polymeric species, L, if one neglects the effect of the excluded volume interactions. The latter assumption is somewhat justified by the fact that decane is not a good solvent for the polymers, as both constitutive monomers are almost insoluble in it. The variation of L with the concentration is reported in Figure 7(b). In the semidilute range, L represents the contour length of the blob. The results obtained in the dilute range show that the polymeric fibrils break under a temperature increase. This effect is in agreement with the theoretical expectations, if one assumes that the fibrils result from the aggregation of monomolecular wires whose length obeys the theory of equilibrium polymers. The latter predicts, in the long chain limit, the following temperature and concentration dependence of the weight-average polymerization degree, DP_W, of the chain:

$$DP_W = 2C^{1/2} \exp(G/2kT) \quad (6)$$

where C is the molar concentration of monomers and G represents the binding free energy that depends not only on the thermodynamics of the bonding between two monomers in a chain, but

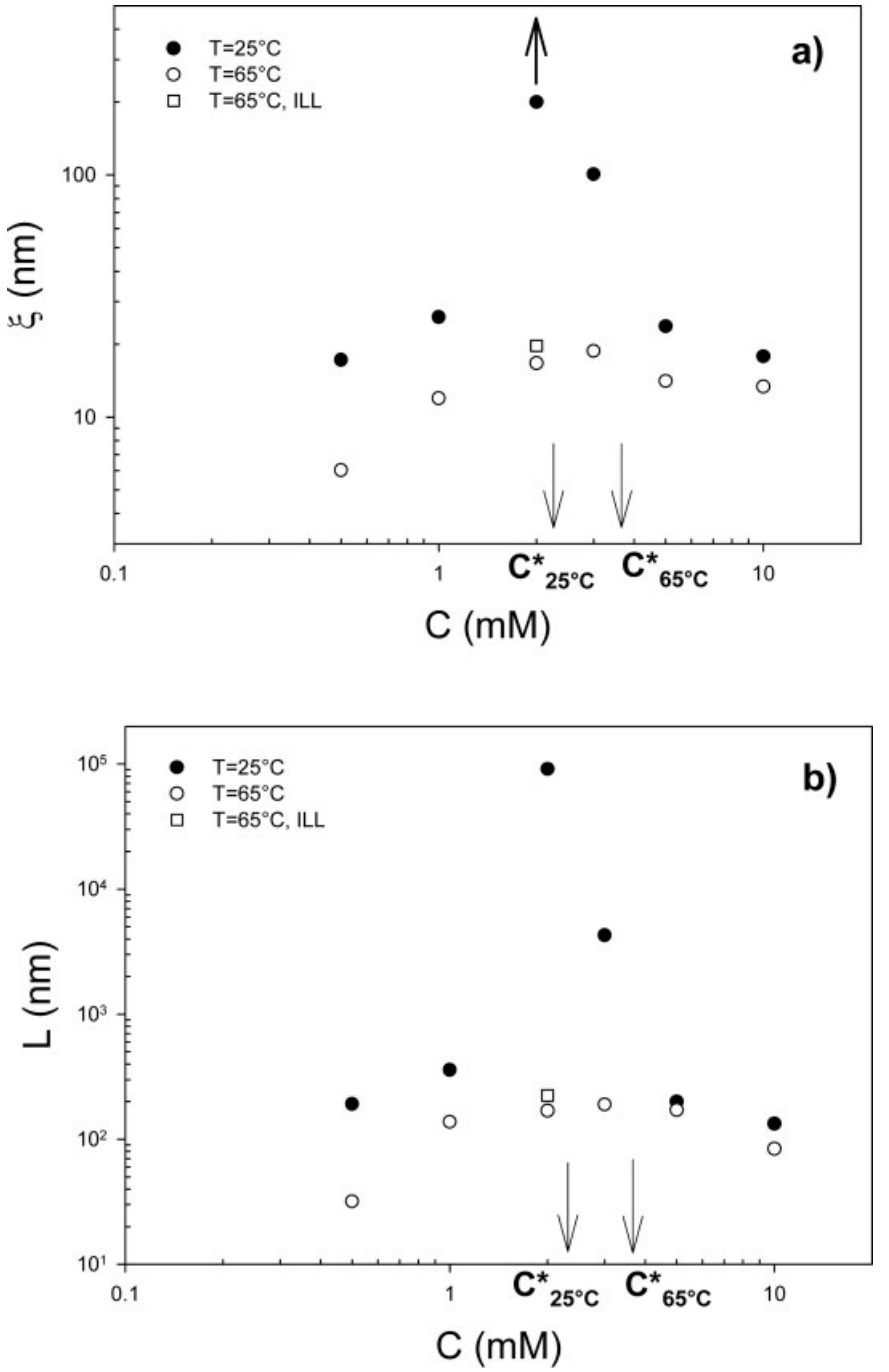

Figure 7. Concentration dependence of (a) the correlation length, ξ, and of (b) the contour length, L, at $T = 25$ °C (●) and 65 °C (○). Data obtained in a previous set at $T = 65$ °C are also reported (□).[38]

also on the solvent type and on the bending rigidity of the chains.[46,47] In the field of giant micelles, G is usually referred to as the end-cap energy. Figure 8 shows a semilog plot of the measured length at a concentration of $C = 1$ mM as a function of $10^3/T$. From the slope of the straight line, one obtains a value of the enthalpic part of the binding free energy, $H = (16 \pm 1)$ kT, that is, (40 ± 2.5) kJ mol^{-1}. In most reported studies on wormlike micelles, the entropic contribution to the binding free energy is neglected. If one makes such an assumption, one can determine the

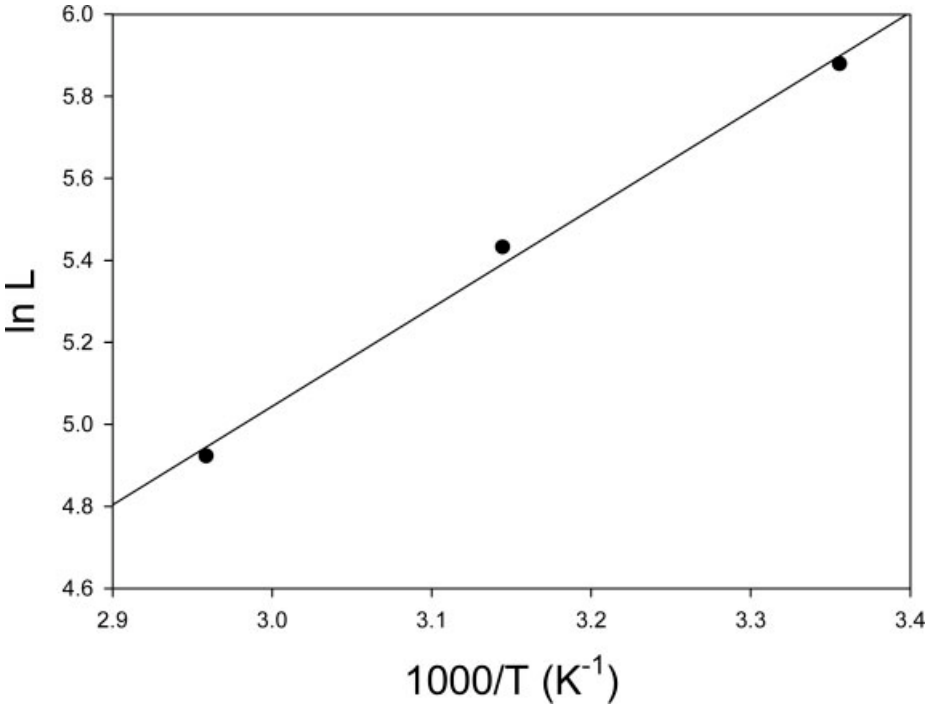

Figure 8. Semi-Log plot of the length, L (in nm), as a function of the ratio $1000/T$ for a $C = 1$ mM solution of $[AA9:BB]_n$ in decane.

weight-average polymerization degree, $DP_{W,chain}$, of a chain from the value of H and using eq 6. Table 1 gives the results obtained in the dilute range at $T = 25$ and 65 °C. In the same Table, we report the values of the weight-average molecular weight, $M_{W,fibril}$, of the fibrils determined from $I(q = 0)$. Estimates of the number of chains, n, per fibril are given, as obtained from $DP_{W,chain}$ and $M_{W,fibril}$, taking for the molecular weight of the monomeric unit the value 1090 g mol^{-1} that corresponds to half the sum of the molecular weights of the biswedge and the bisreceptor units. The values of n are reported in Table 1. The average value is $n = (8 \pm 5)$ chains per fibril, if one neglects the lower value obtained for the shortest fibril ($C = 0.5$ mM and $T = 65$ °C). In the latter case, the long chain limit condition under which eq 6 applies might not be reached. Also, another source of uncertainty arises from neglecting the excluded volume interaction in the determination of the molecular weight of the fibrils.

By combining the measurements of the radius of gyration, R_G, and of the contour length, L, one can obtain an estimate of the persistence length, L_p, from the Benoit–Doty expression derived for a wormlike chain without excluded volume interactions.[48]

$$\langle R_G^2 \rangle = \frac{LL_p}{3} - L_p^2 + \frac{2L_p^3}{L} - \frac{2L_p^4}{L^2}(1 - \exp(-L/L_p)) \quad (7)$$

In the limit $L \gg L_p$, the chain behaves as a Gaussian coil with $R_G^2 = LL_p/3$, and as a rigid rod with $R_G^2 = L^2/12$ for $L \ll L_p$. Table 2 gives data of L_p determined in the dilute regime with eq 7, as a function of the values of L and R_G measured previously. Inspection of Table 2 calls

Table 1. Concentration Dependence in the Dilute Range of $DP_{W,chain}$, of the Apparent Weight–Average Molecular Weight of the Fibrils, $M_{W,fibril}$, and of n, the Number of Chains per Fibril

C (mM)	$DP_{W,chain}$[a]	$M_{W,fibril}$ (g mol^{-1})	n
$T = 25$°C			
0.5	80–220	9.85×10^5	4.1–11
1	114–310	1.84×10^6	5.4–14.8
$T = 65$°C			
0.5	30–80	1.64×10^5	1.9–5.0
1	42–114	7.08×10^5	5.7–15.4
2	60–160	8.71×10^5	5.0–13.3

[a] Values calculated from eq 6 assuming $G = (40 \pm 2.5)$ kJ mol^{-1}.

Table 2. Effect of the Concentration of $[AA9:BB]_n$ Dilute Solutions, C, and of the Temperature on the Contour Length, L, the Radius of Gyration, R_G, and the Persistence Length, L_p

C (mM)	L (nm)	R_G (nm)	L_p (nm)
$T = 65°C$			
0.5	32	10.4	–
1	137	21	12
2	169	29	21
3	190	32.5	23.5
$T = 45°C$			
1	229	27.8	12
$T = 25°C$			
0.5	191	30	18.5
1	358	45	20
2	91400	$\geq$346	4

for two remarks. First, for $C = 0.5$ mM at $T = 65$ °C, the particle behaves as a rigid rod, as shown by the comparison between the calculated value $R_G = L/12^{1/2} = 9.2$ nm and the experimental value of 10.4 nm. Secondly, the very low value of L_p obtained at $C = 2$ mM and $T = 25$ °C is not consistent with the inverse scattering vector at which the scattering curve departs from the q^{-1} behavior for $I(q)$, which strongly suggests a branched conformation of the chain. The average value of L_p inferred from the other data of Table 2 is $L_p = 18 \pm 5$ nm, in agreement with the extents of q^{-1} ranges observed in the scattering curves.

The rather large flexibility of the polymeric fibrils supports the previous conclusion that these fibrils contain few polymeric chains. At this stage, it is not possible to conclude whether the superstructure results from an intra- or an intermolecular stacking of the aromatic rings. The value of the mass per unit length calculated for a fibril formed by intermolecular folding such as that represented in Figure 9(a) is about 40% lower than the experimental one, suggesting that more than two wires are involved in the structure. If the fibrils are ribbons made of intermolecularly stacked wires as represented in Figure 9(b), then a degree of aggregation of about 11 would account for the experimental value of M_l. Thus, both the measurements of $M_{W,fibril}$ and M_l lead to the conclusion that the fibrils consist of few aggregated polymeric chains. Let us note that the determination of M_l is not sensitive to the excluded volume interactions. Figure 9 shows schematically the evolution of the structure of the self-assemblies as the concentration increases at low and high temperature, respectively. At low concentration (e.g., $C = 0.5$ mM at $T = 65$ °C), the polymeric fibril is a short rod with length $L \leq 18$ nm. As the concentration increases, the fibril grows and becomes semiflexible. Upon increasing the concentration further, the scenario depends on the temperature. At $T = 65$ °C, the behavior is that observed for other equilibrium polymers, namely an overlapping of the growing linear chains above C^*. At $T = 25$ °C, the fibrils become interconnected to form highly branched aggregates in the vicinity of C^*. These interconnections are likely to subsist in the semidilute regime.

CONCLUSIONS

The results reported in this study on dispersions of two homoditopic heterocomplementary monomers in decane provide a general description of the structure of the supramolecular polymeric entities formed as a function of concentration and temperature by the $[AA9:BB]_n$ entity (Fig. 1). The section of the polymeric fibrils is found to be $\sim$10 nm^2 from both SANS and cryo-TEM experiments. This value, as well as the mass per unit length, of $M_l \sim 5000$ g mol^{-1} nm^{-1}, suggests that stacking of the aromatic rings occurs, leading to either an intramolecular folding or a lateral aggregation of unfolded monomolecular wires. The persistence length (L_p) of the fibers, inferred from the combined measurements of the radius of gyration and of the contour length, was found to be $\sim$18 nm.

The contour length of the supramolecular aggregates decreases upon increasing temperature according to an Arrhenius law. From this dependence, the enthalpic part of the binding free energy was found to be equal to 16 kT in agreement with the values obtained for other equilibrium polymers that range between 10 and 40 kT.[46,47] The evolution of the structure of the fibrils with concentration depends on the temperature. At $T = 65$ °C, the variation of the correlation length with concentration is similar to that observed for other equilibrium polymer solutions, with a weak increase of the length in the dilute regime and a smooth maximum around the crossover concentration, C^*. This is the behavior expected for linear polymers undergoing a monotonous growth as the concentration increases. At $T = 25$ °C, both SANS and cryo-

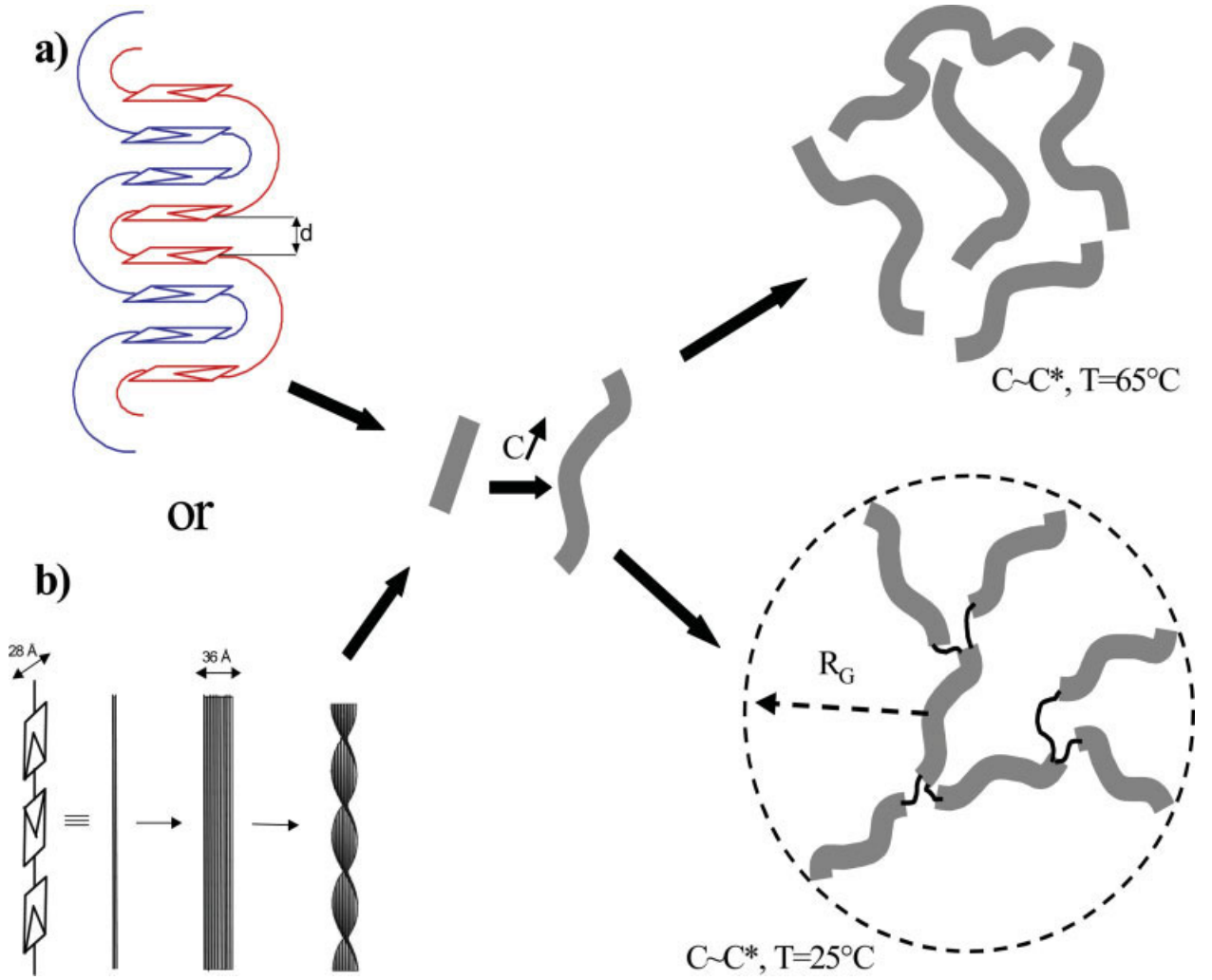

Figure 9. Possible evolution with the concentration of the structure of the fibrillar aggregates formed by the $[AA9:BB]_n$ supramolecular polymer at $T = 25$ and 65 °C. In the representation of the molecular folding consisting of the interpenetration of two chains; d is equal to 3.4 Å (a). The second possibility is an intermolecular stacking of straight monomolecular chains (b). The lateral chains have not been represented. [Color figure can be viewed in the online issue, which is available at www.interscience.wiley.com.]

TEM data show the formation of branched aggregates. The presence of interfiber connections is expected to strongly affect the rheological properties of the semi-dilute solutions of such polymers, as will be discussed in a forthcoming study.

The authors gratefully acknowledge F. Boué for his help during the SANS experiments performed on the spectrometer PACE at LLB-Saclay. In the course of the study are also reported some data obtained in a previous set of measurements carried out at ILL-Grenoble. The cryo-TEM work was performed at the Harnnah and George Krumholz Laboratory for Advanced Microscopy, part of the Technion Project on Complex Fluids, Microstructure, and Macromolecules.

REFERENCES AND NOTES

1. Supramolecular Polymers; Ciferri, A., Ed.; Dekker: New York, 2000.
2. Brunsveld, L.; Folmer, B. J. B.; Meijer, E. W.; Sijbesma, R. P. Chem Rev 2001, 101, 4071.
3. Lehn, J. M. Polym Int 2002, 51, 825.
4. Moore, J. S. Curr Opin Colloid Interface Sci 1999, 4, 108.

5. Paleos, C. M.; Tsiourvas, D. Adv Mater 1997, 9, 695.
6. Sherrington, D. C.; Taskinen, K. A. Chem Soc Rev 2001, 30, 83.
7. Schmuck, C.; Wienand, W. Angew Chem Int Ed Engl 2001, 40, 4363.
8. Proc Natl Acad Sci USA 2002, 99, 8; Special Edition on Self Assembly Processes.
9. Fouquey, C.; Lehn, J. M.; Levelut, A. M. Adv Mater 1990, 2, 254.
10. Prins, L. J.; Reinhoudt, D. N.; Timmerman, P. Angew Chem 2001, 113, 2446.
11. Hirschberg, K.; Brunsveld, J.; Ramzi, A.; Vekemans, J. A. J.; Sijbesma, R. P.; Meijer, E. W. Nature 2000, 38, 2870.
12. Ikkala, O.; ten Brinke, G. Science 2002, 295, 2407.
13. Kotera, M.; Lehn, J. M.; Vigneron, J. P. J Chem Soc Chem Commun 1994, 197.
14. Kotera, M.; Lehn, J. M.; Vigneron, J. P. Tetrahedron 1995, 51, 1953.
15. Lehn, J. M.; Mascal, M.; DeCian, A.; Fischer, J. J Chem Soc Chem Commun 1990, 479.
16. Lehn, J. M.; Mascal, M.; DeCian, A.; Fischer, J. J Chem Soc Perkin Trans 1992, 461.
17. Berl, V.; Schmutz, M.; Krische, M. J.; Khoury, R. G.; Lehn, J. M. Chem—Eur J 2002, 8, 1227.
18. Ikeda, M.; Nobori, T.; Schmutz, M.; Lehn, J. M. Chem—Eur J 2005, 11, 662.
19. Sijbesma, R. P.; Beijer, F. H.; Brunsveld, L.; Folmer, B. J. B.; Hirschberg, J. H. K.; Lange, R. F. M.; Lowe, J. K. L.; Meijer, E. W. Science 1997, 278, 1601.
20. Folmer, B. J. B.; Cavini, E.; Sijbesma, R. P.; Meijer, E. W. Chem Commun 1998, 1847.
21. Lillya, C. P.; Baker, R. J.; Hütte, S.; Winter, H. H.; Lin, Y. G.; Shi, J.; Dickinson, C.; Chien, J. C. W. Macromolecules 1992, 25, 2076.
22. Lee, C. M.; Jariwala, C. P.; Griffin, A. C. Polymer 1994, 35, 4550.
23. Bladon, P.; Griffin, A. C. Macromolecules 1993, 26, 6604.
24. Alexander, C.; Jariwala, C. P.; Lee, C. M.; Griffin, A. C. Makromol Chem Macromol Symp 1994, 77, 283.
25. St. Pourcain, C. B.; Griffin, A. C. Macromolecules 1995, 28, 4116.
26. Choi, I. S.; Li, X.; Simanek, E. E.; Akaba, R.; Whitesides, G. M. Chem Mater 1999, 11, 684.
27. Abed, S.; Boileau, S.; Bouteiller, L.; Lacoudre, N. Polym Bull 1997, 39, 317.
28. He, C.; Lee, C. M.; Griffin, A. C.; Bouteiller, L.; Lacoudre, N.; Boileau, S.; Fouquet, C.; Lehn, J. M. Mol Cryst Liq Cryst 1999, 332, 251.
29. Lortie, F.; Boileau, S.; Bouteiller, L.; Chassenieux, C.; Demé, B.; Ducouret, G.; Jalabert, M.; Laupretre, F.; Terech, P. Langmuir 2002, 18, 7218.
30. Kato, T.; Fujumasa, M.; Fréchet, J. M. J. Chem Mater 1995, 7, 368.
31. Kihara, H.; Fréchet, J. M. J. Liq Cryst 1998, 24, 413.
32. Kihara, H.; Kato, T.; Uryu, T.; Fréchet, J. M. J. Chem Mater 1996, 8, 961.
33. Kato, T.; Kihara, H.; Kumar, U.; Uryu, T.; Fréchet, J. M. J. Angew Chem Int Ed Engl 1994, 33, 1644.
34. Kato, T.; Ihata, O.; Ujiie, S.; Tokita, M.; Watanabe, J. Macromolecules 1998, 31, 3551.
35. Kato, T.; Kubota, Y.; Nakano, M.; Uryu, T. Chem Lett 1995, 1127.
36. Castellano, R. K.; Rudkevich, D. M.; Rebek, J., Jr. Proc Natl Acad Sci USA 1997, 94, 7132.
37. Seto, C. T.; Whitesides, G. M. J Am Chem Soc 1993, 115, 905.
38. Kolomiets, E.; Buhler, E.; Candau, S. J.; Lehn, J. M. Macromolecules 2006, 39, 1173.
39. Bellare, J. R.; Davis, H. T.; Scriven, L. E.; Talmon, Y. J Electron Microsc Tech 1988, 10, 87.
40. Talmon, Y. In Modern Characterization Methods of Surfactant Systems; Binks, B. P. Ed.; Dekker: New York, 1999; Ch. 5, p 147.
41. Danino, D.; Gupta, R.; Satyavolu, J.; Talmon, Y. J Colloid Interface Sci 2002, 249, 180.
42. Danino, D.; Bernheim-Groswasser, A.; Talmon, Y. Colloids Surf A 2001, 113, 183.
43. Zhang, Y.; Schmidt, J.; Talmon, Y.; Zakin, J. J Colloid Interface Sci 2005, 286, 696.
44. Kesselman, E.; Talmon, Y.; Bang, B.; Abbas, S.; Li, Z.; Lodge, T. P. Macromolecules 2005, 38, 6779.
45. des Cloizeaux, J. Macromolecules 1973, 6, 403.
46. Cates, M. E.; Candau, S. J. J Phys Condens Matter 1990, 2, 6869.
47. van der Schoot, P. In Supramolecular Polymers; Ciferri, A., Ed.; CRC Press: Boca Raton, FL, 2005; and references therein.
48. Benoît, H.; Doty, P. J Phys Chem 1953, 57, 958.